

Research Paper

Theoretical Study of the Motion Characteristics of a Variable Length Connecting Rod Mechanism

Jiadui CHEN*, Qinghua LIU, Kai YANG

*Key Laboratory of Advanced Manufacturing Technology
Ministry of Education, Guizhou University*

Guiyang 550025, China

*Corresponding Author e-mail: jdchen1@gzu.edu.cn

The sustainable development of society calls for automobile engines with high efficiency and very low pollutant emission. The variable compression ratio (VCR) technique is one of the effective methods to deal with this issue. Engines with variable length connecting rod (VLEs) yield higher efficiency than other VCR engines. This paper focuses on a variable length connecting rod mechanism that achieves a VCR by changing the positions of the bottom dead center (BDC) and the top dead center (TDC) (controlled by the rotation of the eccentric sleeve) relative to the crankshaft. A kinematic model is also proposed to calculate and analyze the motion characteristics of the variable length connecting rod mechanism. The effects of eccentric size and eccentric phase on the piston motion, the TDC and BDC positions, the stroke length, the crank angles at TDC and BDC, and the compression ratio are studied in detail. It is found that the piston exhibits good motion characteristics with proper eccentric size and eccentric phase, and the compression ratio can be adjusted by varying the eccentric phase with proper eccentric size. A comparison between the proposed mechanism with another mechanism is also conducted. Therefore, this work can serve as a necessary reference for designing, analyzing, and optimizing VLEs.

Key words: variable length connecting rod engine; variable stroke; variable compression ratio; kinematic model; piston movement process.

1. INTRODUCTION

Since the invention of internal combustion engines (ICEs) by Nicolaus Otto in 1876 [1, 2], cars have become the primary means of transportation. In recent years, global car ownership has been soaring rapidly with the development of the global economy. The mass use of cars brings convenience to human beings; however, it also creates a serious energy crisis and environmental issues. According to the research, most of the fossil fuel is consumed by engine vehicles, and the primary factor leading to urban air pollution is exhaust emission from inter-

nal combustion engine vehicles [3]. Hence, higher fuel economy standards and emission standards have been implemented or put forward by many countries [4]. A new fuel economy standard stating that the maximum fuel consumption must be 5 l per 100 km is implemented this year in China [5]. In Europe, cars cannot emit more than 60 g of CO₂ per kilometer until 2025 [6]. In the United States, starting in 2025, the fuel consumption of light-duty vehicles must meet the requirement of 23 km/l on average [2]. Therefore, future engines must be able to operate efficiently in all working conditions to meet increasingly strict fuel consumption and emission standards.

Several measures have been undertaken to raise fuel economy and thermal efficiency, and reduce exhaust emissions of automobiles. The variable compression ratio (VCR) technology, the lean-burn principle, and the downsizing of turbocharging engines have been considered the most efficient technologies to improve thermal efficiency and reduce fuel consumption. The downsizing of turbocharging engines can supply more power in high-load conditions and reduce the pumping and mechanical loss [7]. However, a knock phenomenon appears when the boost pressure is greater than a fair value in spark-ignition engines; thus, engines suffer from poor efficiency due to a relatively low CR under light load conditions. Leaner mixture and lower combustion temperature are the main characteristics of the lean-burn principle. One of the typical examples of the lean-burn principle is homogeneous charge compression ignition (HCCI). However, there are two fundamental drawbacks in HCCI: the difficulty in combustion phasing control and a narrow operation range [8].

In the VCR technology, the compression ratio (CR) of a fuel engine can be easily controlled according to its operating conditions, leading to enhanced engine efficiency, fuel economy and reduced engine emission [9, 10]. The VCR technology enables VCR engines to achieve higher thermal efficiency at a low power level by running at a large CR and also to prevent knocking with a low CR at a high power level. VCR can also be integrated with other engine technologies. In combination with the downsizing of turbocharging, VCR can greatly enhance the engine performance by varying the CR according to the best requirements for the CR under both large load and light load conditions. VCR can avoid misfire under light load conditions using a large CR and prevent knocking under heavy load conditions by decreasing the CR [5]. Therefore, VCR can extend the working range of HCCI engines and also improve their controllability at combustion phasing. Due to the advantages of VCR, numerous VCR mechanisms have been proposed by car manufacturers and engine researchers. The FEV company developed a VCR engine with the crankshaft bearing installed in an eccentrically mounted carrier. The piston's TDC position in the cylinder can be changed by rotating the eccentrically mounted carrier, leading to a VCR [11, 12]. The Nissan VCR system is a multi-link mechanism that con-

nects a control linkage system to an actuator shaft between the connecting rod and the crankshaft [13, 14]. The Saab VCR engine uses a novel method to dynamically change the position of the cylinder head, thus resulting in a VCR [15]. Engines developed by Ford can vary the CR by a valve or secondary piston to change the volume of the combustion chamber [16]. Gomecsys patented a new type of VCR engine, in which a moveable crankpin driven by a large gear can form an eccentric sleeve around the conventional crankpin in the VCR system. The VCR system changes the engine CR by varying the position of the moveable crankpin [17]. Honda developed a VCR engine with a variable piston height [18]. HIYOSHI *et al.* [9] developed a new VCR mechanism that can vary the engine CR by changing the position of the added triangle. KADOTA *et al.* [19] proposed a dual-piston VCR engine that can change the CR by adjusting the TDC position of the piston by a spring and a hydraulic system. KLEEBERG *et al.* [20] proposed a VCR mechanism with an eccentric carrier placed between the piston and the small end of the connecting rod. The VCR mechanism could modify the CR by changing the angular displacement of the eccentric carrier. YAMIN and OZCAN [21] studied a variable stroke engine and its compression ratio. JIANG and SMITH [22] designed a multi-link mechanism with a variable displacement to develop a VCR engine.

The VCR characteristics, the fuel economy, thermal efficiency, and exhaust emission of VCR engines have been extensively studied. Very few researchers have theoretically discussed the piston movement characteristics of VCR engines. However, a reasonable geometric design of a VCR system can provide a better adjustment performance of the variable compression ratio. Therefore, different approaches have been proposed to realize a variable compression ratio.

JIANG and SMITH [22] proposed a design method for the multi-link mechanism of a VCR engine and studied its piston motion, displacement, stroke length, compression ratio, combustor volume, and other characteristics. YANG and LIN [5] studied the piston movement process of a VCR mechanism with an eccentric sleeve and discussed the effects of the bore-to-stroke ratio and the eccentric phase on the piston motion, the compression ratio, and the Atkinson effect. RUFINO and FERREIRA [23] studied the motion laws of a VCR engine with a multi-link mechanism and presented a new strategy to determine the movement laws as the functions of the combustion chamber capacity and the CR.

In the present paper, the movement characteristics of a VLE, such as piston acceleration, velocity, and displacement are analyzed in detail. This work also presents a mathematical model to calculate the dead center position and the compression ratio. It also discusses the effects of the eccentric size and the eccentric phase.

The remaining part of this paper is divided into five sections: Sec. 2 introduces the kinematic model of the VLE piston. Section 3 presents a mathematical

model to calculate the dead center position and CR of the VLE. Section 4 discusses the effects of the eccentric size and the eccentric phase. A comparison between the proposed mechanism with other mechanisms is shown in Sec. 5. A summary of the study is presented in Sec. 6.

2. KINEMATIC MODEL

The geometry of the VLE mechanism is displayed in Fig. 1. The structure and working principle of the VCR mechanism are introduced in [24] (l_{OA} is the radius of the crank (R), l_{AB} is the length of the connecting rod (l), and l_{BC} is the eccentric size (e)). The kinematic model is composed of displacement, velocity, and acceleration equations. First, the piston displacement equation was developed according to the geometry of the VLE mechanism. The piston velocity equation was then obtained by taking the derivative of the piston displacement equation. Finally, the piston acceleration equation was obtained by taking the derivative of the piston velocity equation.

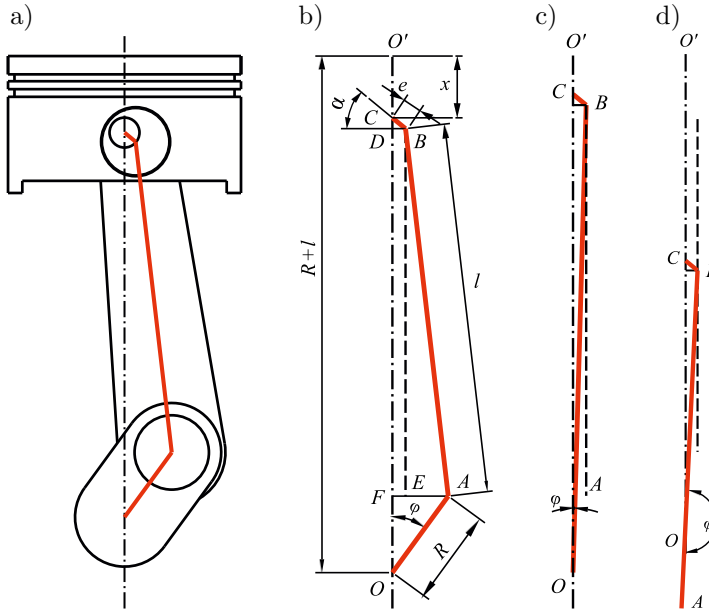


FIG. 1. The geometry of the VLE.

When the crank rotates clockwise, the height of the piston l_{OC} can be calculated as:

$$(2.1) \quad l_{OC} = l_{OF} + l_{FD} + l_{DC}.$$

According to the geometric relationship, l_{OF} can be calculated as:

$$(2.2) \quad l_{OF} = l_{OA} \cos \varphi = R \cos \varphi,$$

where φ is the crank angle, and l_{FD} can be calculated as:

$$(2.3) \quad l_{FD} = l_{EB} = \sqrt{l_{AB}^2 - l_{AE}^2} = \sqrt{l_{AB}^2 - (l_{FA} - l_{FE})^2} \\ = \sqrt{l_{AB}^2 - (l_{FA} - l_{DB})^2},$$

where

$$(2.4) \quad l_{FE} = l_{DB},$$

$$(2.5) \quad l_{FA} = l_{OA} \sin \varphi = R \sin \varphi,$$

$$(2.6) \quad l_{DB} = l_{BC} \cos \alpha = e \cos \alpha,$$

where α is the eccentric phase of the eccentric sleeve.

Equation (2.3) can be rewritten as:

$$(2.7) \quad l_{FD} = \sqrt{l_{AB}^2 - (l_{FA} - l_{DB})^2} = \sqrt{l^2 - (R \sin \varphi - e \cos \alpha)^2}.$$

l_{DC} can be expressed as:

$$l_{DC} = l_{BC} \sin \alpha = e \sin \alpha.$$

Hence, Eq. (2.1) can be rewritten as:

$$(2.8) \quad l_{OC} = R \cos \varphi + \sqrt{l^2 - (R \sin \varphi - e \cos \alpha)^2} + e \sin \alpha.$$

Let assume that the piston of the VLE has the same peak height as the piston of a compression ratio engine (CRE). Hence, the piston displacement (x) can be calculated as:

$$(2.9) \quad x = l_{OO'} - l_{OC} = R + l - R \cos \varphi - \sqrt{l^2 - (R \sin \varphi - e \cos \alpha)^2} - e \sin \alpha.$$

The piston velocity (v) can be obtained by differentiating Eq. (2.9):

$$(2.10) \quad v = \frac{dx}{dt} = \frac{dx}{d\varphi} \cdot \frac{d\varphi}{dt} = \omega R \left[\sin \varphi + \frac{(R \sin \varphi - e \cos \alpha) \cos \varphi}{\sqrt{l^2 - (R \sin \varphi - e \cos \alpha)^2}} \right].$$

The piston acceleration of the VLE can be obtained as:

$$(2.11) \quad a = \frac{dv}{dt} = \frac{dv}{d\varphi} \cdot \frac{d\varphi}{dt} = \omega^2 R \left[\cos \varphi + \frac{R \cos^2 \varphi - R \sin^2 \varphi + e \sin \varphi \cos \alpha}{\sqrt{l^2 - (R \sin \varphi - e \cos \alpha)^2}} + \frac{R (R \sin \varphi - e \cos \alpha)^2 \cos^2 \varphi}{\sqrt{[l^2 - (R \sin \varphi - e \cos \alpha)^2]^3}} \right].$$

Therefore, when the geometric parameters of the VLE mechanism are known, and both the crank speed and the crank angle are given, the piston motion for the total revolution of the crankshaft could be calculated according to the above equations.

3. DEAD CENTER POSITION AND CR CALCULATION

In order to study the variations of the stroke length and the CR of the VLE, the dead center position was calculated. The VLE mechanism could be considered as an offset slider-crank mechanism with an eccentricity of $e \cos \alpha$. According to the motion characteristics of an offset slider-crank mechanism, when the crank and the connecting rod are connected in a straight line, the VLE piston is located at the TDC (Fig. 1c). When the crank and the connecting rod are connected in a straight line, the VLE piston is located at the BDC (Fig. 1d). Therefore, the TDC position and its corresponding crank angle (φ_{TDC}) can be calculated as:

$$(3.1) \quad x_{\text{TDC}} = l + R - \sqrt{(l + R)^2 - (e \cos \alpha)^2} - e \sin \alpha,$$

$$(3.2) \quad \varphi_{\text{TDC}} = \sin^{-1} \frac{e \cos \alpha}{R + l}.$$

According to Fig. 1d, the BDC position and its corresponding crank angle (φ_{BDC}) can be calculated as:

$$(3.3) \quad x_{\text{BDC}} = l + R - \sqrt{(l - R)^2 - (e \cos \alpha)^2} - e \sin \alpha,$$

$$(3.4) \quad \varphi_{\text{BDC}} = 180 + \sin^{-1} \frac{e \cos \alpha}{l - R}.$$

Therefore, the stroke length (S) can be obtained

$$(3.5) \quad S = x_{\text{BDC}} - x_{\text{TDC}} = \sqrt{(l + R)^2 - (e \cos \alpha)^2} - \sqrt{(l - R)^2 - (e \cos \alpha)^2}.$$

The CR can be calculated as:

$$(3.6) \quad \varepsilon = 1 + \frac{V_S}{V_C},$$

where V_S is the piston displacement, and V_C is the compression chamber volume. V_S can be calculated as:

$$(3.7) \quad V_S = \frac{\pi d^2}{4} S = \frac{\pi d^2}{4} \left(\sqrt{(l+R)^2 - (e \cos \alpha)^2} - \sqrt{(l-R)^2 - (e \cos \alpha)^2} \right),$$

where d is the cylinder diameter.

According to Fig. 2, V_C can be calculated as:

$$(3.8) \quad \begin{aligned} V_C &= V_{C0} + \frac{\pi d^2}{4} x_{TDC} \\ &= V_{C0} + \frac{\pi d^2}{4} \left(l + R - \sqrt{(l+R)^2 - (e \cos \alpha)^2} - e \sin \alpha \right), \end{aligned}$$

where V_{C0} is the compression chamber volume of the CRE.

Now, substituting Eqs. (3.7) and (3.8) into Eq. (3.6):

$$(3.9) \quad \begin{aligned} \varepsilon &= 1 + \frac{\frac{\pi d^2}{4} \left(\sqrt{(l+R)^2 - (e \cos \alpha)^2} - \sqrt{(l-R)^2 - (e \cos \alpha)^2} \right)}{V_{C0} + \frac{\pi d^2}{4} \left(l + R - \sqrt{(l+R)^2 - (e \cos \alpha)^2} - e \sin \alpha \right)} \\ &= \frac{V_{C0} + \frac{\pi d^2}{4} \left(l + R - e \sin \alpha - \sqrt{(l-R)^2 - (e \cos \alpha)^2} \right)}{V_{C0} + \frac{\pi d^2}{4} \left(l + R - \sqrt{(l+R)^2 - (e \cos \alpha)^2} - e \sin \alpha \right)}. \end{aligned}$$

If the cylinder is a regular cylindrical cavity as shown in Fig. 2, V_C can be expressed as:

$$(3.10) \quad \begin{aligned} V_C &= V_{C0} + \frac{\pi d^2}{4} x_{TDC} \\ &= \frac{\pi d^2}{4} H + \frac{\pi d^2}{4} \left(l + R - \sqrt{(l+R)^2 - (e \cos \alpha)^2} - e \sin \alpha \right) \\ &= \frac{\pi d^2}{4} \left(H + l + R - \sqrt{(l+R)^2 - (e \cos \alpha)^2} - e \sin \alpha \right), \end{aligned}$$

where H is the compression chamber height of the CRE.

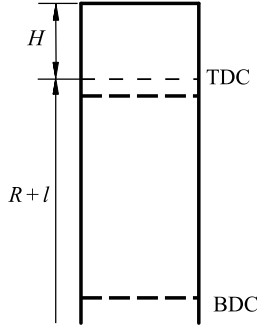


FIG. 2. Schematic diagram of the cylinder.

Now, substituting Eqs. (3.7) and (3.10) into Eq. (3.6)

$$\begin{aligned}
 (3.11) \quad \varepsilon &= 1 + \frac{\sqrt{(l+R)^2 - (e \cos \alpha)^2} - \sqrt{(l-R)^2 - (e \cos \alpha)^2}}{H+l+R - \sqrt{(l+R)^2 - (e \cos \alpha)^2} - e \sin \alpha} \\
 &= \frac{H+l+R - \sqrt{(l-R)^2 - (e \cos \alpha)^2} - e \sin \alpha}{H+l+R - \sqrt{(l+R)^2 - (e \cos \alpha)^2} - e \sin \alpha}.
 \end{aligned}$$

4. EFFECTS OF ECCENTRIC SIZE AND ECCENTRIC PHASE

An eccentric sleeve is a key component of a VLE to achieve a variable compression ratio. The eccentric size and eccentric phase of an eccentric sleeve greatly affect the piston motion, the positions of TDC and BDC, the compression ratio, the crank angles at TDC and BDC, and the stroke length. In order to study the effects of the eccentric size and the eccentric phase, a 400 cc engine was taken as the baseline to reveal the motion characteristics of the VLE piston. Table 1 presents the main parameters of the engine.

Table 1. Major baseline engine parameters.

| Item | Parameter |
|------------------------|-----------|
| Displacement [cc] | 400 |
| Compression ratio | 10.5 |
| Cylinder diameter [mm] | 81 |
| Stroke [mm] | 77.5 |
| Crank radius [mm] | 38.75 |
| Connecting rod [mm] | 145.5 |
| Speed [rpm] | 5800 |

4.1. Influence on piston motion

The piston movement process is generally affected by both the eccentric size (e) and the eccentric phase (α) according to Eqs. (2.9)–(2.11).

Figure 3 exhibits how the piston displacement changed with the eccentric phase. It is noticeable that when the eccentric phase decreased, both BDC and TDC declined in the same direction with clockwise rotation of the eccentric sleeve. This indicates that the stroke length and the compression chamber volume might also change. When the eccentric phase changed, the crank angle locations corresponding to TDC and BDC also changed. It signifies that the change in the eccentric phase changed TDC, BDC, the stroke length, and the crank angles at TDC and BDC.

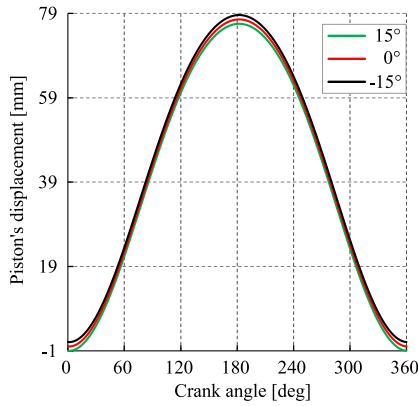


FIG. 3. Influence of the eccentric phase on the piston displacement.

Figure 4 displays the change in the piston displacement with respect to the eccentric size. It is evident that when the eccentric size increased, both BDC

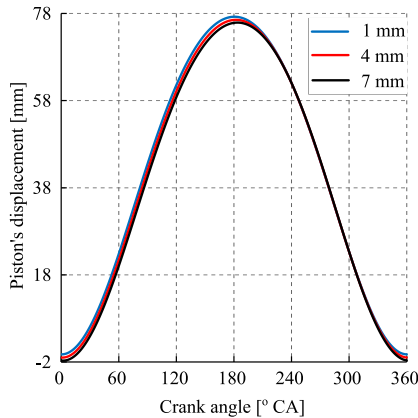


FIG. 4. Influence of the eccentric size on the piston displacement.

and TDC positions were lowered. Similar to Fig. 3, both BDC and TDC moved in the same direction. It is also noticeable that the influence of the eccentric size on the piston displacement during the downward motion of the piston was greater than that during the upward motion of the piston.

Figure 5 shows how the velocity profile of the piston changed with the eccentric size at 1500 rpm. It is noticeable that all profiles had the same shape. Before the crest of the profile, the piston velocity decreased with the increase of the eccentric size. However, the piston velocity increases with the increase of the eccentric size between the crest and trough of the profile. Therefore, the piston velocity decreased with the increase of the eccentric size during the intake and exhaust strokes and increased with the increase of the eccentric size during the compression and expansion strokes.

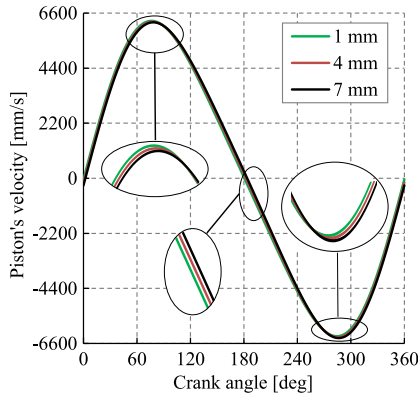


FIG. 5. Influence of the eccentric size on the piston velocity.

Figure 6 exhibits how the piston velocity changed with the eccentric phase at 1500 rpm. It is clear that all profiles had the same shape. Similar to Fig. 5,

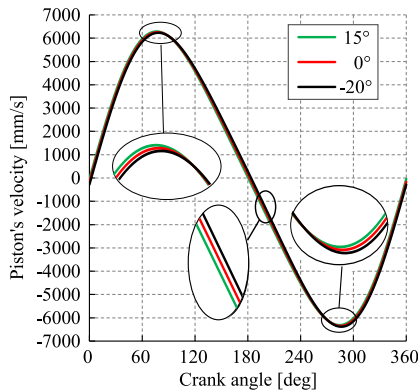


FIG. 6. Influence of the eccentric phase on the piston velocity.

before the crest of the profile, the piston velocity decreased with the decrease of the eccentric phase. The piston velocity increased with the increase of the eccentric phase between the crest and trough of the profile; however, the difference between the curves at the same crank angle was very small.

Figure 7 expresses the change in the piston acceleration with respect to the eccentric size at 1500 rpm. The piston acceleration profile was a u-shaped curve in an engine operating cycle (similar to that of the CRE [5]). In the intake and exhaust strokes, the piston acceleration (absolute values) increased with the increase of the eccentric size and decreased with the increase of the eccentric size in the compression and expansion strokes.

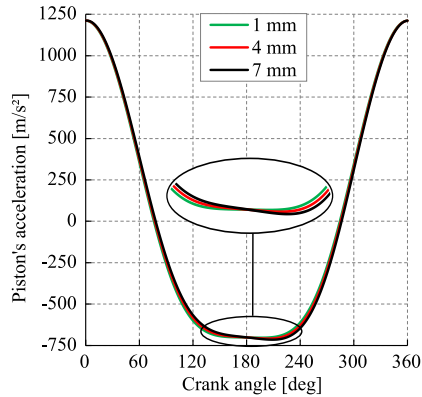


FIG. 7. Influence of the eccentric size on the piston acceleration.

Figure 8 reveals how the piston acceleration changed with the eccentric phase. The shape of the profile in Fig. 8 is very similar to that in Fig. 7. The

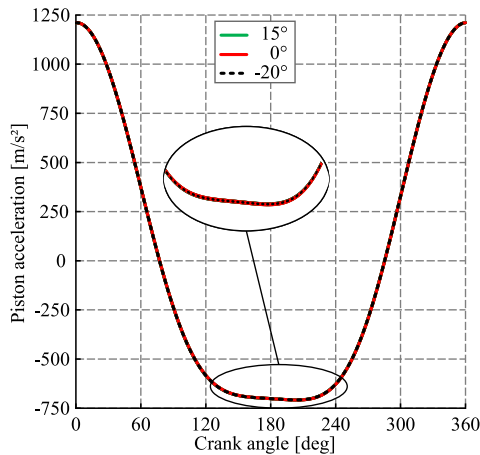


FIG. 8. Effect of the eccentric phase on the acceleration profile of the piston.

effect of the eccentric phase on the piston acceleration was small. The eccentric phase with the same absolute value had the same effect on the piston acceleration as stated by Eq. (2.11).

4.2. Influence on TDC and BDC positions

Figure 9 displays the changes in the BDC and TDC positions with respect to the eccentric size. It is evident that the value of the TDC position was negative, indicating that the TDC position relative to the crankshaft axis was higher than that of the CRE. When the eccentric size increased, both TDC and BDC positions increased, and the change rate of the TDC position was greater than that of the BDC position. Therefore, the stroke length increased as the eccentric size increased.

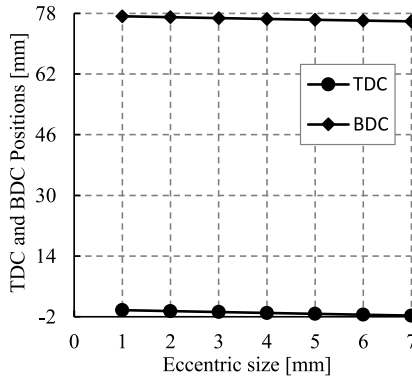


FIG. 9. Effect of the eccentric size on TDC and BDC positions.

Figure 10 exhibits how the positions of TDC and BDC changed with the eccentric phase. It is noticeable that when the eccentric sleeve turned clockwise

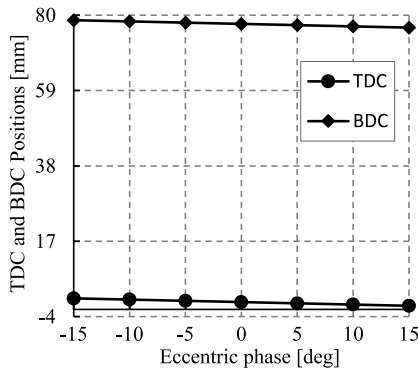


FIG. 10. Effect of the eccentric phase on TDC and BDC positions.

(eccentric phase increased from -15° to 15°), both TDC and BDC positions relative to the crankshaft axis increased, and the change rate of the TDC position also increased. However, the change rate of the BDC position first gradually increased and then decreased, and the maximum value was obtained at 0° . When the eccentric phase was greater than 0° , the value of the TDC position was smaller than 0° , which signifies that the TDC position of the VCR was higher than that of the CRE.

4.3. Influence on the crank angles at TDC and BDC

The eccentric size of the connecting rod and the eccentric phase of the eccentric sleeve created a phase shift at TDC, which indicates that the crank angle at TDC did not occur at exactly $\varphi = 0^\circ$ crank angle (CA). The profiles of the crank angle at TDC with respect to the eccentric size and the eccentric phase are displayed in Figs. 11 and 12, respectively. It is evident that the relation between the crank angle at TDC and the eccentric size of the connecting rod was almost linear (Fig. 9). When the eccentric size increased from 1 mm to 7 mm,

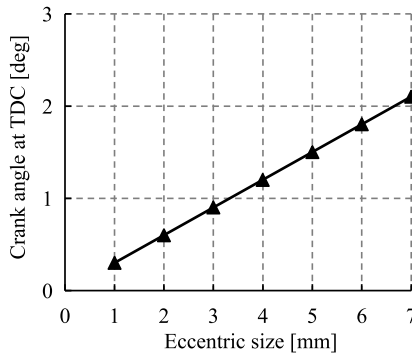


FIG. 11. Effect of the eccentric size on the crank angle at the TDC.

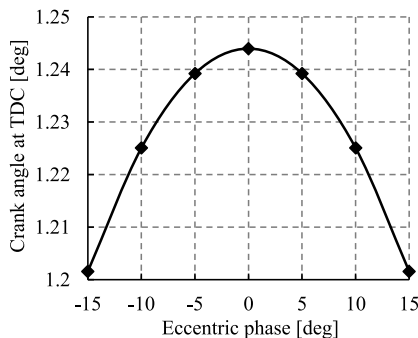


FIG. 12. Effect of the eccentric phase on the crank angle at the TDC.

the crank angle at TDC increased from 0.3° CA to 2.1° CA. The curve of the crank angle at TDC with respect to the eccentric phase was symmetrical, and when the eccentric phase was $\alpha = 0^\circ$, the curve of the crank angle at TDC reached the maximum value of 1.24° CA.

Due to the configuration of the mechanism, the BDC also did not occur at $\varphi = 180^\circ$ CA; thus, the crank angle at the BDC also shifted. Figure 13 reveals how the crank angle at the BDC changed with the eccentric size. It is clear that the relation between the crank angle at the BDC and the eccentric size of the connecting rod was almost linear. When the eccentric size increased from 1 mm to 7 mm, the crank angle at the BDC increased from 180.52° CA to 183.63° CA. The effect of the eccentric size on the crank angle at the BDC was greater than that at the TDC. Figure 14 presents how the crank angle at the BDC behaved with the varying eccentric phase. The profile of the influence of the eccentric phase on the crank angle at the BDC was a symmetrical curve, and the peak of the curve (182.15° CA) appeared at the eccentric phase of $\alpha = 0^\circ$. The effect of the eccentric phase on the crank angle at the BDC was greater than that at the TDC.

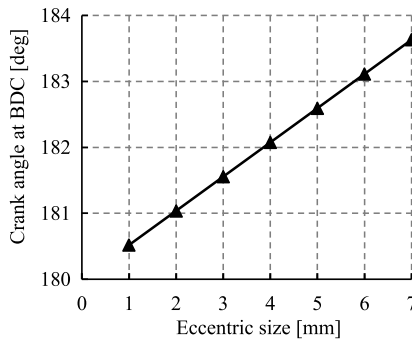


FIG. 13. Effect of the eccentric size on the crank angle at the BDC.

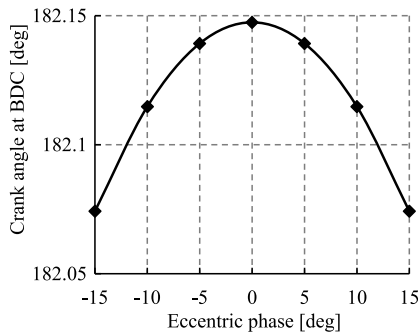


FIG. 14. Effect of the eccentric phase on the crank angle at the BDC.

4.4. Influence on the stroke length and the CR

Figure 15 exhibits how the stroke length changed with the eccentric size. The relation between the stroke length and the eccentric size was nonlinear. When the eccentric size increased from 1 mm to 7 mm, the stroke length increased from 77.5 mm to 77.59 mm (a variation of 0.09 mm). Therefore, the variation of the eccentric size had less influence on the stroke length. The profile of the influence of the eccentric phase on the stroke length was a symmetrical curve (Fig. 16). When the eccentric phase was $\alpha = 0^\circ$, the curve of the stroke length reached the peak value of 77.5315 mm. Similar to the eccentric size, the effect of the eccentric phase on the stroke length was very small. When the eccentric sleeve rotated clockwise, the eccentric phase varied from -15° to 0° , and the variation of the stroke length was only 0.021 mm.

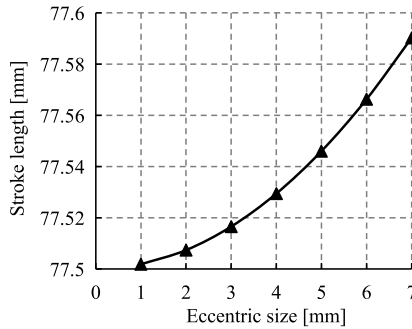


FIG. 15. Effect of the eccentric size on the stroke length.

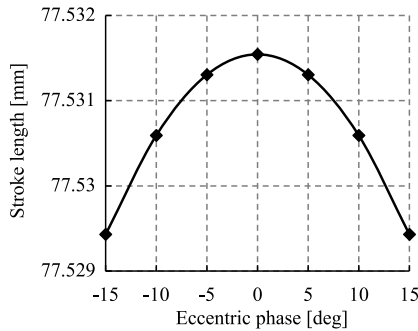


FIG. 16. Effect of the eccentric phase on the stroke length.

The profiles of the CR with respect to the eccentric size and the eccentric phase are displayed in Figs. 17 and 18, respectively. When the eccentric size increased from 1 mm to 7 mm, the CR increased from 10.81 to 12.99. When the eccentric phase varied from -15° to 15° , the CR increased from 9.39 to 11.82.

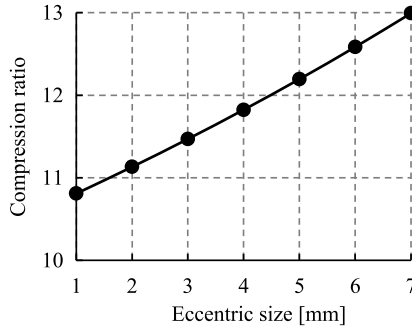


FIG. 17. Effect of the eccentric size on the CR.

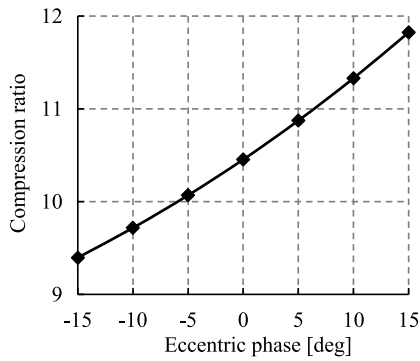


FIG. 18. Effect of the eccentric phase on the CR.

Therefore, an appropriate CR could be obtained by choosing a reasonable eccentric size and adjusting the eccentric phase during engine operation.

5. COMPARISON WITH ANOTHER MECHANISM

One of the main concerns in the design of the proposed mechanism is to compare the characteristics with another VCR mechanism. Table 2 shows the compa-

Table 2. Comparison of the characteristics between the proposed mechanism and reference [22].

| Item | JIANG and SMITH [22] | Proposed mechanism |
|--|----------------------|--------------------|
| Piston's displacement [mm] | 103–247 | 108–185 |
| Piston's velocity [mm/deg] | –1.15–1.25 | –0.71–0.7 |
| Piston's acceleration [mm/deg ²] | –0.021–0.021 | –0.009–0.015 |
| Stroke length [mm] | 117.9–135.3 | 77.5–77.59 |
| Compression ratio | 8–13.8 | 7.3–19 |

parison of the characteristics between the proposed mechanism and the mechanism presented in [22]. The data from [22] in Table 2 are obtained from the graphs given in [22], and the data are the maximum and minimum value of the curve in each graph. In order to facilitate comparison, the data of the proposed mechanism such as the zero of displacement, the units of velocity and acceleration have been transformed. In addition, the CR values for the proposed mechanism are the result of the eccentric size of 7 mm and the eccentric phase changes from -35° to 35° .

In Table 2, we can see that for the displacement and stroke in [22] both the value and range of variation are greater than those of the proposed mechanism, which means that the size of the mechanism in [22] is larger than that of the proposed mechanism. A characteristic to be considered in this analysis is the piston's velocity and acceleration. Excessive speed and acceleration will bring vibration and shock to the engine, resulting in the unstable operation of the engine. It can be seen in Table 2 that both the values (including absolute values) and variation ranges of the piston's velocity and acceleration of the proposed mechanism are smaller than those of the mechanism in [22]. We know that the larger the compression ratio, the better the performance of the engine. Moreover, the larger the variation range of CR, the more reasonable adjustment of CR can be made according to the working condition of the VCR engine. Therefore, the engine is always in the best working state. As can be seen in Table 2, the maximum value and variable range of the CR of the proposed mechanism are greater than those of the mechanism in [22], while the minimum value of the CR is smaller than that of the mechanism in [22].

6. CONCLUSION

VCR is one of the promising technologies that could handle the increasingly strict emission regulations. It is reported that the piston movement process significantly affects engine performance in many ways. VLEs can offer higher efficiency, lower fuel consumption, and lower pollutant emission than VCR engines. The present paper presented a kinematic model of the VLE piston and a mathematical calculation model of the dead center position and the CR. The effects of the eccentric size and the eccentric phase on the piston motion, the positions at TDC and BDC, the crank angles at TDC and BDC, the stroke length, and the CR were discussed. The main observations are presented below:

- 1) The eccentric size and the eccentric phase had great effects on the motion characteristics of the piston. The efficiency and performance of the VLE could be improved by choosing the proper eccentric size and eccentric phase.

- 2) The positions of TDC and BDC relative to the crankshaft axis increased with the increase of the eccentric size; however, the change rate of the TDC position was greater than that of the BDC position. Therefore, the stroke length increased as the eccentric size increased.
- 3) When the eccentric sleeve turned clockwise from negative to positive angles, both TDC and BDC positions relative to the crankshaft axis increased. The change rate of the TDC position continuously increased; however, the change rate of the BDC position first increased and then decreased, making the profile of the influence of the eccentric phase on the stroke length an inverted U-shaped symmetric curve.
- 4) The crank angles at TDC and BDC did not, respectively, occur at $\varphi = 0^\circ$ CA and $\varphi = 180^\circ$ CA. The crank angles at TDC and BDC increased with the increase of the eccentric size. However, the profiles of the influence of the eccentric phase on the crank angles at TDC and BDC were inverted U-shaped symmetric curves with the peak at 0° .
- 5) The CR could be varied by changing the eccentric size and the eccentric phase. An appropriate CR could be obtained by choosing a reasonable eccentric size and adjusting the eccentric phase during engine operation.
- 6) Compared with another mechanism, the proposed mechanism can achieve a larger range of CR adjustment and has a smaller piston's displacement, velocity and acceleration.

FUNDING

This research was funded by the Youth Science and Technology Talent Growth Project by the Department of Education of Guizhou Province (Grant numbers: KY [2017]106 and KY(2018)112) and the Science and Technology Foundation of Guizhou Province (Grant number: [2020]1Y262 and [2020]1Y232).

REFERENCES

1. GANESAN V., *Internal Combustion Engines*, McGraw Hill, India, 2012.
2. HOELTGEBAUM T., SIMONI R., MARTINS D., Reconfigurability of engines: A kinematic approach to variable compression ratio engines, *Mechanism and Machine Theory*, **96**(Part 2): 308–322, 2016, doi: 10.1016/j.mechmachtheory.2015.10.003.
3. HEYWOOD J., MACKENZIE D. [Eds], *On the road toward 2050: potential for substantial reductions in light-duty vehicle energy use and greenhouse gas emissions*, Massachusetts Institute of Technology, pp. 301–313, 2015, <https://energy.mit.edu/wp-content/uploads/2015/12/MITEL-RP-2015-001.pdf>.
4. Feng D.Q., Wei H.Q., PAN M.Z., Comparative study on combined effects of cooled EGR with intake boosting and variable compression ratios on combustion and emis-

- sions improvement in a SI engine, *Applied Thermal Engineering*, **131**: 192–200, 2018, doi: 10.1016/j.applthermaleng.2017.11.110.
5. YANG S., LIN J.S., A theoretical study of the mechanism with variable compression ratio and expansion ratio, *Mechanics Based Design of Structures and Machines*, **46**(3): 267–284, 2018, doi: 10.1080/15397734.2017.1332526.
 6. WESTERLOH M., TWENHÖVEL S., KOEHLER J., SCHUMACHER W., Worldwide electrical energy consumption of various HVAC systems in BEVs and their thermal management and assessment, *SAE Technical Paper*, 2018-01-1190, 2018, doi: 10.4271/2018-01-1190.
 7. CLENCI A.C., DESCOMBES G., PODEVIN P., HARA V., Some aspects concerning the combination of downsizing with turbocharging, variable compression ratio, and variable intake valve lift, *Proceedings of the Institution of Mechanical Engineers, Part D: Journal of Automobile Engineering*, **221**(10): 1287–1294, 2007, doi: 10.1243/09544070jauto449.
 8. MINGFA Y., ZHAOLEI Z., HAIFENG L., Progress and recent trends in homogeneous charge compression ignition (HCCI) engines, *Progress in Energy and Combustion Science*, **35**(5): 398–437, 2009, doi: 10.1016/j.pecs.2009.05.001.
 9. HIYOSHI R., AOYAMA S., TAKEMURA S., USHJIMA K., SUGIYAMA T., A study of a multiple-link variable compression ratio system for improving engine performance, *SAE Technical Paper*, 2006-01-0616, 2006, doi: 10.4271/2006-01-0616.
 10. TAKAHASHI N., AOYAMA S., MOTEKI K., HIYOSHI R., A study concerning the noise and vibration characteristics of an engine with multiple-link variable compression ratio mechanism, *SAE Technical Paper*, 2005-01-1134, 2005, doi: 10.4271/2005-01-1134.
 11. ASTHANA S., BANSAL S., JAGGI S., KUMAR N., A comparative study of recent advancements in the field of variable compression ratio engine technology, *SAE Technical Paper*, 2016-01-0669, 2016, doi: 10.4271/2016-01-0669.
 12. MANE P., PENDOVSKI D., SONNEN S., UHLMANN A., HENAUX D., BLUM R., SHARMA V., Coupled dynamic simulation of two stage Variable Compression Ratio (VCR) connecting rod using virtual dynamics, *SAE International Journal of Advances and Current Practices in Mobility*, **1**(1): 38–44, 2019, doi: 10.4271/2019-26-0031.
 13. SHELBY M.H., LEONE T.G., BYRD K.D., WONG F.K., Fuel economy potential of variable compression ratio for light duty vehicles, *SAE International Journal of Engines*, **10**(3): 817–831, 2017, doi: 10.4271/2017-01-0639.
 14. KOJIMA S., KIGA S., MOTEKI K., TAKAHASHI E., MATSUOKA K., Development of a new 2L gasoline VC-turbo engine with the world's first variable compression ratio technology, *SAE Technical Paper* 2018-01-0371, 2018, doi: 10.4271/2018-01-0371.
 15. ROMERO C., HENAO CASTAÑEDA E., Developing small variable compression ratio engines for teaching purposes in an undergraduate program, *SAE Technical Paper* 2019-01-0331, 2019, doi: 10.4271/2019-01-0331.
 16. SHAIK A., MOORTHI N.S.V., RUDRAMOORTHY R., Variable compression ratio engine: A future power plant for automobiles – an overview, *Proceedings of the Institution of Mechanical Engineers, Part D: Journal of Automobile Engineering*, **221**(9): 1159–1168, 2007, doi: 10.1243/09544070JAUTO573.
 17. WITTEK K., GEIGER F., ANDERT J., MARTINS M., OLIVEIRA M., An overview of VCR technology and its effects on a turbocharged DI engine fueled with ethanol and gasoline, *SAE Technical Paper* 2017-36-0357, 2017, doi: 10.4271/2017-36-0357.

18. SHI H., AL MUDRAA S., JOHANSSON B., Variable compression ratio (VCR) piston – design study, *SAE Technical Paper*, 2019-01-0243, 2019, doi: 10.4271/2019-01-0243.
19. KADOTA M., ISHIKAWA S., YAMAMOTO K., KATO M., KAWAJIRI S., Advanced control system of variable compression ratio (VCR) engine with dual piston mechanism, *SAE International Journal of Engines*, **2**(1): 1009–1018, 2009, doi: 10.4271/2009-01-1063.
20. KLEEGERG H., TOMAZIC D., DOHMEN J., WITTEK K., BALAZS A., Increasing efficiency in gasoline powertrains with a two-stage variable compression ratio (VCR) system, *SAE Technical Paper* 2013-01-0288, 2013, doi: 10.4271/2013-01-0288.
21. YAMIN J.A.A., OZCAN H., Second-law analysis of an LPG-powered 4-stroke SI engine under variable stroke length and compression ratio, *International Journal of Exergy*, **8**(2): 113–127, 2011, doi: 10.1504/IJEX.2011.038514.
22. JIANG S., SMITH M.H., Geometric parameter design of a multiple-link mechanism for advantageous compression ratio and displacement characteristics, *SAE Technical Paper* 2014-01-1627, 2014, doi: 10.4271/2014-01-1627.
23. RUFINO C.H., FERREIRA J.V., Kinematics of a variable stroke and compression ratio mechanism of an internal combustion engine, *Journal of the Brazilian Society of Mechanical Sciences and Engineering*, **40**: Article number: 476, 2018, doi: 10.1007/s40430-018-1396-x.
24. CHEN J., WANG B., LIU D., YANG K., Study on the dynamic characteristics of a hydraulic continuous variable compression ratio system, *Applied Sciences*, **9**(21): 4484, 2019, doi: 10.3390/app9214484.

Received May 27, 2021; accepted version November 14, 2021.



Copyright © 2022 J. Chen *et al.*

This is an open-access article distributed under the terms of the Creative Commons Attribution-ShareAlike 4.0 International (CC BY-SA 4.0 <https://creativecommons.org/licenses/by-sa/4.0/>) which permits use, distribution, and reproduction in any medium, provided that the article is properly cited, the use is non-commercial, and no modifications or adaptations are made.